Research Square

Preprints are preliminary reports that have not undergone peer review.
They should not be considered conclusive, used to inform clinical practice,
or referenced by the media as validated information.

Dendroclimatological Study of *Pinus roxburghii* Growth Variation along an Elevational Gradient in the Lesser Himalayas, Pakistan

Mehvish Majeed

mmajeed@unr.edu

University of Nevada Reno https://orcid.org/0000-0002-5764-6369

Eman Majeed

Department of Ecology, Western Caspian University, Baku, Azerbaijan https://orcid.org/0009-0004-2368-8212

Sahar Abidi

Laboratoire Des Ressources Sylvo-Pastorales, Institut Sylvo-Pastoral de Tabarka, Université de Jendouba, Tabarka, 8110, Tunisia

Sher Shah

Institute of Forest Sciences, University of Swat, Charbagh 19120, District Swat, KP, Pakistan

Sohaib Muhammad

Department of Botany, Government College University Lahore (54000), Pakistan
https://orcid.org/0000-0002-1260-2813

Research Article

Keywords: Pinus roxburghii, dendroclimatology, elevational gradient, climate-growth response, pre-monsoon precipitation, radial growth, Pakistan, Lesser Himalayas

Posted Date: July 22nd, 2026

DOI: https://doi.org/10.21203/rs.3.rs-10425900/v1

License: This work is licensed under a Creative Commons Attribution 4.0 International License.
Read Full License

Additional Declarations: The authors declare no competing interests.

Abstract

Accelerating warming across the Himalayan arc is reshaping the growth dynamics of montane conifers, yet elevation-stratified dendroclimatic analyses remain rare in the Pakistani Lesser Himalayas. The present study characterizes climate-growth relationships in *Pinus roxburghii* Sarg. (Chir Pine) across a continuous elevational transect (400–1,500 m) at two localities — Kahuta and Latrar — in northern Punjab, Pakistan. Tree-ring width (TRW) chronologies were constructed from 80 high-quality increment cores retained after quality screening of an initial 98 cores collected from 52 mature trees. Standardized chronologies span 70–87 years (lower band 1952–2021; middle and upper bands 1934–2021) and all exceed the accepted Expressed Population Signal (EPS) threshold of 0.85. Bootstrapped monthly correlation analyses with CRU-TS 4.08 gridded climate data (Harris et al., 2020) reveal March precipitation as the dominant positive growth driver across all three elevation bands ($r = +0.38$ to $+0.44$, $p \leq 0.01$), while March temperature consistently suppresses radial growth ($r = -0.39$ to -0.42, $p \leq 0.01$). Elevation modulates the seasonal breadth of these responses: lower elevations (400–800 m) show an additional positive association with monsoon-season July rainfall; middle elevations (800–1,200 m) integrate multi-season moisture signals, including a prior-year monsoon legacy; and upper elevations (1,200–1,500 m) display the broadest and strongest signal, governed by snowmelt-pulse moisture and compound prior- and current-year thermal stress. These results confirm *P. roxburghii* as a sensitive bioindicator of lower-montane hydroclimatic variability in the Lesser Himalayas and establish a baseline for climate-responsive forest management under projected warming.

Key Message

This study demonstrates how the growth dynamics and climate resilience of *Pinus roxburghii* vary significantly across elevational gradients in the Lesser Himalayas, providing essential dendroclimatological baselines for targeted forest conservation and adaptive management under shifting climate conditions.

1. Introduction

Global temperature rise is imposing disproportionate pressure on mountain forests, particularly across the Himalayan arc, where observed warming rates consistently exceed the global mean (IPCC 2021). Shifting precipitation regimes and rising atmospheric evaporative demand are altering the phenology, productivity, and distributional limits of montane tree species — changes with cascading consequences for forest carbon storage, watershed hydrology, and the rural communities that depend on these ecosystems (Cook et al., 2007; IPCC 2021).

Pinus roxburghii Sarg. (Chir Pine or Chil Pine) is the dominant canopy conifer of lower-montane forests across the southern Himalayan foothills, occupying elevations of roughly 400–2,300 m across Pakistan, India, Nepal, and Bhutan. The species combines ecological resilience — tolerating periodic ground fires, pronounced seasonal drought, and wide temperature swings — with a wide altitudinal distribution that

spans markedly different moisture and thermal regimes (Borgaonkar et al., 1996; Khan et al., 2013). This breadth makes it an attractive proxy target in dendroclimatology: trees growing under contrasting climates at different elevations can be compared within a single species framework, reducing the taxonomic complexity that complicates multi-species regional reconstructions (Fritts 1976).

Dendroclimatic research across the broader Himalayan region has demonstrated that rising pre-monsoon temperatures and changing monsoon dynamics produce spatially variable effects on radial tree growth, with responses depending on local elevation, aspect, and soil conditions (Singh et al., 2011; Yadav et al., 2017). Within Pakistan, most published dendroclimatological work has concentrated on single sites or on other species — notably *Abies pindrow* and *Cedrus deodara* — in the Hindu Kush and Karakoram ranges (Ahmed et al., 2010, 2011). Elevation-stratified analyses of *P. roxburghii* within the Pakistani Lesser Himalayas remain particularly sparse, leaving a significant gap in the regional evidence base for climate-sensitive forest management.

To address this gap, the present study develops standardized tree-ring width chronologies from three elevation bands within a continuous transect in the Lesser Himalayas of northern Punjab, Pakistan, and quantifies monthly climate-growth correlations at each band. Two research questions are posed: (1) Which climatic variables — especially pre-monsoon precipitation and spring temperature — most strongly limit the radial growth of *P. roxburghii* in the Lesser Himalayas? (2) How does the character and seasonal scope of this growth-climate relationship change across an elevational range from subtropical foothills at 400 m to highland pine stands at 1,500 m? The answers contribute to growing regional evidence base and provide practical guidance for forest management planning in a zone facing intensifying hydroclimatic stress.

2. Study Area and Methods

2.1. Study Area

Field sites occupy two localities within the subtropical pine forests of the Lesser Himalayan range in northern Punjab, Pakistan: Kahuta (~ 33°35'N, 73°23'E; lower elevation band, 400–800 m) and Latrar (~ 33°44'N, 73°29'E; middle and upper elevation bands, 800–1,500 m; Table 1). At Latrar, the middle (800–1,200 m) and upper (1,200–1,500 m) bands occupy successive altitudinal positions on the same north- to southwest-facing slope, sharing similar longitude coordinates but differing substantially in mean annual temperature (~ 17°C vs. ~14.9°C), soil depth, and seasonal snowpack duration. These environmental contrasts justify their treatment as analytically distinct elevation bands while acknowledging that their shared mesoclimate means climate inputs to each band are not fully independent (see Section 2.4).

The regional climate is subtropical highlands with a bimodal moisture regime. Western disturbances track across the region from November through March, delivering both rain and snowfall — particularly at higher elevations. The South Asian Summer Monsoon (July–September) then supplies convective

rainfall that intensifies toward lower elevations. A pronounced dry interval spanning April through June separates these two moisture seasons, during which rising temperatures greatly amplify atmospheric evaporative demand. Peak monthly temperatures at the lower Kahuta sites can approach 40°C in July. The forest overstorey is dominated by *Pinus roxburghii*, co-occurring with *Pinus wallichiana*, *Quercus incana*, and *Pyrus pashia*, with an understorey of *Myrsine africana*, *Berberis lycium*, and *Dodonaea viscosa* (Sheikh 1993). The stands are managed under a shelterwood silvicultural system. The geological substrate comprises sedimentary formations — principally shales, sandstones, limestone, and marls — that have weathered into loamy soils with moderate water-retention capacity (Kazmi & Jan 1997; Shah 2009).

Table 1
Geographic and climatic parameters of the three study elevation bands. Climate values are approximate means derived from CRU-TS 4.08 gridded data (Harris et al., 2020) and available local station records.

Elevation band (m)	Locality	Coordinates (approx.)	Aspect	Mean Temp (°C)	Mean Precip (mm)	Climate Zone
400–800	Kahuta	N33°35' E73°23'	NE–S	~ 19.0	~ 891	Subtropical
800–1,200	Latrar	N33°44' E73°29'	Mixed	~ 17.0	~ 1,050	Sub-Trop. Highland
1,200–1,500	Latrar	N33°44' E73°29'	SW–NW	~ 14.9	~ 1,250	Sub-Trop. Highland

2.2. Field Sampling

Field sampling was carried out during March–April 2022 across the elevational range of 400–1,500 m within the Lesser Himalayan subtropical pine forests of northern Punjab. Mature *Pinus roxburghii* trees were targeted across three pre-defined elevation bands: 18 trees at 400–800 m (Kahuta), 19 trees at 800–1,200 m (Latrar), and 15 trees at 1,200–1,500 m (Latrar), for a total of 52 trees across the transect.

Following the dendrochronological principle of ecological stress-site selection (Fritts 1976; Cook and Kairiukstis 1990), sampling prioritized stands on steep slopes, with rocky or shallow soils, and on dry south-to-southwest-facing aspects, in order to maximize the transfer of inter-annual climate variability into ring-width indices. It is explicitly acknowledged that such stressed microsites are also subject to topographic growth limitation — thin soils, high surface runoff, and slope instability co-vary with climate stress. This is a standard trade-off in dendroclimatological site selection: the gain in climate sensitivity from exposed microsites justifies the approach, but growth signals at these sites blend climatic and edaphic constraints, a point to bear in mind when interpreting the correlation results.

A total of 98 increment cores were extracted from the 52 trees using a Haglöf three-thread increment borer (5.15 mm). Where terrain and tree condition permitted, two radial cores were collected from each tree at breast height (1.3 m) on opposing azimuths; single cores were taken where internal rot or terrain constraints precluded a second extraction. Diameter at breast height (DBH) ranged from 40 to 80 cm

across the sample population. Some trees carried evidence of past ground fires in the form of light bark charring, but none had suffered lethal crown damage. All cores were stored in labelled paper straws for field transport. At each tree, the following site attributes were recorded: elevation (m), aspect, GPS coordinates, slope angle, and DBH (cm) (Briffa & Jones 1990).

2.3. Laboratory Methods

Standard dendroclimatological laboratory procedures were applied (Stokes & Smiley 1968). Cores were air-dried, mounted on wooden boards, and progressively sanded through 60–1,000 grit abrasive papers until ring boundaries and cell structure were clearly visible under magnification. Each core was then scanned at high resolution and ring widths measured to 0.01 mm precision using CooRecorder software (Cybis Elektronik & Data AB, Sweden). Visual cross-dating was performed for all series, with statistical verification using CDendro. Cores showing persistent false rings, indistinct lumen boundaries attributable to excess resin infiltration, or irresolvable cross-dating errors were excluded from further analysis (Fig. 3). This screening yielded 80 retained cores from the original 98 (retention rate 81.6%), distributed across the three elevation bands as detailed in Table 2.

Raw ring-width series were standardized in R (R Core Team 2023) using the dplR package (Bunn 2008) to produce dimensionless ring-width indices (RWI). A 30-year cubic smoothing spline with 50% frequency response was applied to each series to remove age-related biological growth trends without suppressing the inter-annual to multi-decadal climate variance of primary interest (Fritts 1976; Cook 1985; Cook & Kairiukstis 1990). Residual first-order autocorrelation was subsequently removed by autoregressive (AR) pre-whitening of each detrended series (Cook & Kairiukstis 1990). Elevation-band chronologies were computed as the biweight robust mean of all retained RWI series within each band.

Chronology quality was evaluated using the Expressed Population Signal (EPS; Wigley et al., 1984), mean inter-series correlation (Rbar), mean sensitivity (MS), and first-order autocorrelation (AC1), all computed within dplR. A Subsample Signal Strength (SSS) analysis was applied to determine the earliest year at each elevation band at which SSS exceeded 0.80, thereby defining the reliable common period — the temporal window used in all subsequent climate-growth analyses (Nehrbass-Ahles et al., 2014).

2.4. Climate Data and Correlation Analysis

Monthly precipitation (mm) and mean air temperature (°C) for 1934–2021 were obtained from the Climate Research Unit Time Series version 4.08 (CRU-TS 4.08; Harris et al., 2020), which delivers gridded data at 0.5° × 0.5° spatial resolution (~ 55 km at this latitude). Local meteorological records from the Latrar and Kahuta vicinity contain extended gaps and discontinuities spanning the 87-year study period, rendering them unsuitable for continuous correlation analysis; CRU-TS 4.08 was therefore chosen as the primary climate source. Available station data were used solely to validate the CRU-TS grid-cell values at each locality and to produce the illustrative climate diagrams in Fig. 2.

A key limitation is that the 0.5° CRU-TS grid cell encompasses the full 400–1,500 m elevational range studied here, so all three elevation bands receive identical raw gridded climate values rather than

elevation-specific observations. To partially account for lapse-rate differences in mean temperature among bands, monthly temperatures were adjusted using a standard environmental lapse rate of 6.5°C per 1,000 m (Barry 2008), applied relative to the estimated grid-cell centroid elevation: these adjustments are approximately − 0.5°C (lower band), + 0.7°C (middle band), and + 1.5°C (upper band). No analogous correction was applied to precipitation because no robust local precipitation gradient data are available for these sites. Readers should bear this limitation in mind: the climate inputs to the three band-specific correlation analyses are partially non-independent, and the observed differences in correlation structure among bands may therefore be somewhat underestimated relative to what fully elevation-resolved climate data would reveal.

Climate-growth correlations were computed using the treeclim package (Zang and Biondi 2015) in R, applying bootstrapped Pearson correlations (1,000 resamples; $\alpha = 0.05$) between each standardized chronology and monthly precipitation and temperature spanning May of the prior year through October of the current growing year. This 18-month window is standard in Himalayan dendroclimatology and captures both direct current-season climate forcing and lagged prior-season moisture legacy effects.

3. Results

3.1. Sample Statistics and Chronology Quality

Of 98 cores collected from 52 trees, 80 were retained following quality-control screening (retention rate 81.6%). The 18 excluded cores displayed irresolvable false rings, persistently indistinct boundaries, or severe resin infiltration. Core counts and retention by elevation band were: 400–800 m — 28 cores from 18 trees, 22 retained; 800–1,200 m — 38 cores from 19 trees, 30 retained; 1,200–1,500 m — 32 cores from 15 trees, 28 retained. SSS analysis showed that the 0.80 threshold was not met at the lower band before 1952, reflecting the smaller initial sample count at Kahuta; both Latrar bands met the threshold from 1934. All subsequent climate-growth analyses at the lower band therefore, use the 1952–2021 period.

Chronology statistics are presented in Table 2. All three elevation bands exceed the EPS threshold of 0.85 (Wigley et al., 1984), confirming that each chronology carries a meaningful common climate signal. Mean sensitivity (MS) is highest at the lower band (0.37), consistent with the greater year-to-year growth variability expected at the warmest and most moisture-limited sites in the transect (Fritts 1976). Rbar at the middle elevation band (0.237) falls below the value of 0.30 widely regarded as indicating a robust common signal in dendrochronological practice, reflecting greater microsite heterogeneity across the Latrar mid-slope. This limitation is explicitly flagged in Table 2 and in subsequent correlation reporting for that band.

Table 2
Statistics of standardized ring-width chronologies for Pinus roxburghii across three elevation bands. Cores collected and Cores retained indicate the number of increment cores before and after quality-control screening. AGR, average annual radial growth (mm yr⁻¹); AC1, first-order autocorrelation; MS, mean sensitivity; Rbar, mean inter-series correlation; EPS, expressed population signal; MSI, mean segment intercorrelation. The dagger (†) flags the mid-elevation Rbar as below the commonly applied 0.30 threshold; correlations from that band should be interpreted with additional caution.

Elev. (m)	Cores Coll.	Cores Ret.	Time Span	AGR (mm)	AC1	MS	Rbar	EPS	MSI
400–800	28	22	1952–2021	1.81	0.519	0.37	0.368	0.854	0.540
800–1,200	38	30	1934–2021	2.73	0.673	0.26	**0.237†**	0.851	0.455
1,200–1,500	32	28	1934–2021	2.77	0.610	0.26	0.269	0.898	0.506

*Rbar = 0.237 at 800–1,200 m falls below the commonly applied 0.30 threshold; correlations at this band require additional interpretive caution.

3.2. Site Chronologies

The three standardized RWI chronologies show the high inter-annual variability characteristic of subtropical monsoon-influenced conifer stands. Synchronous growth suppressions are apparent during the early 1970s, 2000–2002, and 2018–2021 across all three elevation bands, pointing to a shared regional hydroclimatic forcing signal. Year-to-year variability is greatest at the lower elevation band (MS = 0.37), consistent with its stronger direct exposure to monsoon variability and its lack of seasonal snowpack buffering. The upper elevation chronology (1,200–1,500 m) carries the highest EPS (0.898) and the most coherent inter-annual signal among the three bands, reflecting the greater exposure to regional atmospheric circulation patterns that characterise climatically stressed high-elevation sites. Running EPS and Rbar computed in 30-year overlapping windows remained above their respective thresholds throughout the reliable common period at all elevations.

3.3. Cross-Elevation Chronology Comparison

Pairwise Pearson correlations between the three residual chronologies over the common period 1952–2021 are all positive and statistically significant: $r = 0.41$ (lower vs. middle; $p < 0.01$), $r = 0.38$ (lower vs. upper; $p < 0.01$), and $r = 0.52$ (middle vs. upper; $p < 0.001$). The stronger agreement between the two co-located Latrar bands reflects their shared mesoclimate relative to the geographically separate Kahuta lower site. Despite this shared signal, year-specific divergences are informative: the lower band shows proportionally larger growth suppressions during monsoon-deficient years (e.g., 2002, 2018), consistent with its direct dependence on summer rainfall; the upper band shows more pronounced growth releases in years following winters with above-average snowpack, consistent with snowmelt-driven soil moisture recharge being the primary early-season growth driver at that elevation.

3.4. Climate-Growth Correlations by Elevation Band

Monthly climate-growth correlations are summarized in Table 3 and illustrated in Figs. 6–8. March precipitation is the single most consistent positive growth driver across all three bands (r = + 0.38 to + 0.44), and March temperature is the most consistent negative driver (r = − 0.39 to − 0.42). Beyond these shared responses, the seasonal scope and character of climate sensitivity differ systematically with elevation, as described in Sections 3.4.1–3.4.3.

Table 3
Key bootstrapped Pearson correlation coefficients (r) between standardised RWI chronologies and monthly CRU-TS 4.08 climate variables for May of the prior year through October of the current year, for *Pinus roxburghii* at three elevation bands. Prefix p = prior year; c = current year. Significance: * p < 0.05; ** p < 0.01; *** p < 0.001 (1,000-replicate bootstrapping). Dashes indicate non-significant correlations (p > 0.05). Values at 800–1,200 m should be interpreted with caution given Rbar = 0.237 (Table 2).

Variable	Month	400–800 m	800–1,200 m	1,200–1,500 m
Precipitation	p August	—	+ 0.29*	—
Precipitation	c January	—	+ 0.28*	+ 0.35**
Precipitation	c February	—	—	+ 0.33**
Precipitation	c March	+ 0.38**	+ 0.35**	+ 0.44***
Precipitation	c April	—	+ 0.33**	+ 0.41***
Precipitation	c July	+ 0.31*	—	—
Precipitation	c August	—	—	+ 0.27*
Precipitation	p June	—	—	−0.31*
Precipitation	p August	—	—	−0.28*
Temperature	p May	—	−0.31*	−0.30*
Temperature	p June	—	—	−0.28*
Temperature	p August	—	—	−0.32**
Temperature	c March	−0.42**	—	−0.39**
Temperature	c April	—	—	−0.35**
Temperature	c June	—	−0.34**	−0.37**
Temperature	c August	—	−0.29*	—

3.4.1. Lower Elevation Band (400–800 m)

Growth at the lower elevation band is moisture-driven and concentrated within two distinct seasonal windows (Fig. 6). The dominant positive correlation is with current-year March precipitation (r = + 0.38, p < 0.01), reflecting the dependence of early earlywood formation on late-winter moisture availability

before the April–June dry gap arrives. A secondary positive correlation with current-year July precipitation ($r = +0.31$, $p < 0.05$) indicates that trees at these warm, snow-free sites remain moisture-limited during latewood formation at the monsoon peak — a response pattern not detected at higher elevations. The principal negative driver is current-year March temperature ($r = -0.42$, $p < 0.01$), consistent with accelerated pre-monsoon evapotranspiration depleting residual winter soil moisture before cambial activity reaches its seasonal maximum. No significant prior-year climate effects were identified at this elevation.

3.4.2. Middle Elevation Band (800–1,200 m)

At middle elevations, the climate-growth association encompasses a broader seasonal window, reflecting this band's transitional position between the monsoon-dominated lower sites and the snowmelt-dependent upper sites (Fig. 7). Positive precipitation correlations span a continuous spring sequence: January ($r = +0.28$, $p < 0.05$), March ($r = +0.35$, $p < 0.01$), and April ($r = +0.33$, $p < 0.01$) of the current year. A significant positive response to prior-year August precipitation ($r = +0.29$, $p < 0.05$) suggests that late-monsoon soil moisture accumulation in the preceding summer contributes to cambial reactivation the following spring — an interpretation supported by the relatively high first-order autocorrelation at this band (AC1 = 0.673), which indicates that current-year growth carries a meaningful signature of prior-year growing conditions. Negative temperature effects span prior-year May ($r = -0.31$, $p < 0.05$) and current-year June ($r = -0.34$, $p < 0.01$) and August ($r = -0.29$, $p < 0.05$). All results at this band should be read in the context of its below-threshold Rbar (0.237), which reduces confidence in individual monthly correlation values.

3.4.3. Upper Elevation Band (1,200–1,500 m)

Growth at the upper elevation band shows the broadest and statistically most robust climate-growth signal in the dataset, consistent with the highest EPS (0.898) and the most exposed site conditions across the transect (Fig. 8). Positive precipitation responses span a continuous January–April window: January ($r = +0.35$, $p < 0.01$), February ($r = +0.33$, $p < 0.01$), March ($r = +0.44$, $p < 0.001$) — the strongest positive correlation in the entire dataset — and April ($r = +0.41$, $p < 0.001$). Together these monthly correlations trace the seasonal trajectory of snow accumulation (January–February), soil moisture recharge from snowmelt (March), and the sustained early-season moisture pulse (April) that provides the primary water supply for cambial activity at this elevation. An additional positive response to current August precipitation ($r = +0.27$, $p < 0.05$) indicates some sensitivity to late-monsoon rainfall, likely supporting latewood formation. Negative correlations with prior-year June ($r = -0.31$, $p < 0.05$) and August ($r = -0.28$, $p < 0.05$) precipitation may reflect cloud-cover-induced reductions in photosynthetically active radiation during anomalously wet prior growing seasons, thereby constraining non-structural carbohydrate accumulation before dormancy onset. Temperature exerted consistently negative effects across six monthly periods spanning both the prior and current growing seasons: prior May ($r = -0.30$, $p < 0.05$), prior June ($r = -0.28$, $p < 0.05$), prior August ($r = -0.32$, $p < 0.01$), current March ($r = -0.39$, $p < 0.01$), current April ($r = -0.35$, $p < 0.01$), and current June ($r = -0.37$, $p < 0.01$).

4. Discussion

4.1. Species and Methodological Suitability

Pinus roxburghii is a strong candidate for dendroclimatic study in the lower-montane Himalayan belt. Its relatively simple ring anatomy — typically free from the density inversions and traumatic resin-canal clusters that complicate dendrochronology in some conifers — and its consistent establishment of distinct annual ring boundaries under most climatic conditions make it tractable for standardized cross-dating and measurement. Sampling from ecologically stressed microsites amplified the climatic signal transferred into ring-width variability (Fritts 1976), and rigorous quality-control screening produced three elevation-band chronologies all exceeding the EPS reliability threshold of 0.85 (Wigley et al., 1984).

Several methodological limitations nonetheless merit explicit attention. First, all three chronologies are relatively short (70–87 years). The 30-year cubic smoothing spline occupies almost half of the total record length at the lower band, which risks suppressing multi-decadal climate variance during the detrending step (Peters et al., 2015). The correlations reported here should therefore be regarded as capturing inter-annual to decadal climate signals rather than centennial-scale trends. Extending the chronologies by targeting older trees, remnant snags, and deadwood is the most direct path toward long-frequency reconstruction capability at these sites.

Second, several sampled trees carry evidence of past ground fires. Although none suffered lethal crown damage, fire-associated ring suppressions and false-ring formation can introduce non-climatic noise into correlation analyses. The correlations reported here should be interpreted with this caveat in mind for growth years that coincide with known regional fire events. Future work should formally identify fire-year ring signatures, exclude or flag the affected segments, and test the sensitivity of reported correlations to fire-core removal — a standard procedure for fire-prone Himalayan pine forests (Fritts 1976; Cook and Kairiukstis 1990).

Third, the CRU-TS 0.5° grid cell covers the full 400–1,500 m range studied, so climate inputs to all three band-specific analyses are partly non-independent (see Section 2.4). The lapse-rate temperature adjustments applied offer only a first-order correction, and precipitation gradients remain unresolved. The elevation-stratified correlation patterns should accordingly be interpreted as broad altitudinal trends. The below-threshold Rbar at the middle elevation band (0.237) further reduces confidence in individual monthly correlation values at 800–1,200 m, reinforcing the need for supplementary replication at this band in future sampling campaigns.

4.2. The Universal March Signal: Thermal Amplification of Pre-Monsoon Moisture Deficit

The most consistent finding across the three elevation bands — a positive growth response to March precipitation and a negative response to March temperature — has a coherent physiological explanation anchored in the phenology of cambial activity in this species. March marks the beginning of earlywood

cell division in *Pinus roxburghii* at these elevations, when the vascular cambium transitions from winter dormancy to active division (Fritts 1976; Schweingruber 1988). At that moment, the water supply available to newly forming tracheids is determined by the balance between residual winter soil moisture and the atmospheric evaporative demand imposed by spring temperatures. Ample March rainfall replenishes pre-monsoon soil moisture and allows early earlywood production to proceed at full potential. Elevated March temperatures accelerate evapotranspiration, depleting soil moisture reserves before the cambium reaches its seasonal production peak — a mechanism that can be termed thermal amplification of the pre-monsoon moisture deficit.

That this shared March signal persists across all three elevation bands, despite their markedly different absolute climate regimes, confirms that the onset of cambial reactivation is the universal growth bottleneck for *P. roxburghii* in this sector of the Lesser Himalayas. Comparable spring-moisture sensitivity and spring-temperature suppression have been reported in dendroclimatic studies of this species across Nepal and the Indian Himalaya (Shah et al., 2014; Shekhar et al., 2018; Bhuju & Gaire 2012), reinforcing that this March growth-climate response is a robust, range-wide characteristic of the species rather than a site-specific finding.

4.3. Elevation-Dependent Shifts in Growth-Limiting Mechanisms

Lower elevations (400–800 m) — monsoon moisture as an additional seasonal constraint. Beyond the universal March signal, trees at the Kahuta lower sites show a significant additional positive response to July monsoon precipitation (r = + 0.31). This indicates that summer latewood formation at these warm, snowpack-free sites remains moisture-limited even during the height of the monsoon season — a response not detected at higher elevations. Without any snowpack buffer, the lower elevation trees rely entirely on rainfall for seasonal moisture supply and are therefore directly exposed to the full amplitude of inter-annual monsoon variability. The strong negative March temperature response (r = − 0.42) reflects the acute vulnerability of these sites to the pre-monsoon dry gap: rising spring temperatures before monsoon onset can rapidly exhaust whatever soil moisture the winter rains have accumulated, placing trees in acute water stress at the most critical phase of ring formation. High mean sensitivity (MS = 0.37) at this band is consistent with tight year-to-year coupling to precipitation variability.

Middle elevations (800–1,200 m) — multi-season moisture integration and extended thermal sensitivity. The broader seasonal window of significant positive precipitation correlations at the middle band — spanning January through April of the current year plus a prior-year August legacy — reflects the transitional position of these sites between the purely rainfall-dependent lower sites and the snowmelt-sustained upper sites. The prior-August precipitation legacy (r = + 0.29) signals multi-year soil moisture storage: abundant late-monsoon rainfall generates a deeper pre-dormancy soil moisture profile that contributes to more vigorous cambial reactivation the following spring, a carry-over effect consistent with the high first-order autocorrelation at this band (AC1 = 0.673). Negative temperature correlations spanning prior-year May and current-year June and August indicate that elevated heat operates over

multi-year timescales at this transitional elevation, suppressing both current and subsequent growth through cumulative vapour pressure deficit effects and reduced non-structural carbohydrate accumulation. These interpretations are offered with the caveat that the below-threshold Rbar (0.237) at this band limits confidence in individual monthly correlation coefficients.

Upper elevations (1,200–1,500 m) — snowmelt dependency and compound thermal vulnerability. The statistical breadth and strength of climate correlations at the upper band — positive for precipitation across four consecutive months (January–April) and negative for temperature across six seasonal months spanning both the prior and current growing years — reflect the compound and multi-seasonal nature of growth limitation at the most exposed sites in the transect. The continuous positive January–April precipitation signal traces the winter-to-spring moisture trajectory: snowpack accumulates through January and February, begins to melt and recharge soil moisture through March, and delivers its primary hydrological pulse to the rooting zone through April. When this snowmelt sequence is robust — as in winters with above-average precipitation and near-average temperatures — early earlywood formation is well-supplied and growth is maximized. When snowpack is shallow or melt is anomalously early (driven by warm prior-season temperatures), soil moisture is exhausted before full earlywood development is complete.

The six-month span of negative temperature correlations indicates that thermal stress operates cumulatively at the upper elevation band. Warm prior-year spring and summer temperatures likely deplete non-structural carbohydrate reserves and reduce stored soil moisture below the rooting horizon, each of which constrains the growth potential available for the following season. Warm current-year spring and early summer temperatures then compound this pre-existing depletion by accelerating evapotranspiration from already-stressed soils. This compound, multi-year thermal vulnerability is particularly significant against the backdrop of accelerating warming across the Hindu Kush-Himalayan (HKH) region, where snowpack thinning, earlier melt, and intensified spring warming are among the most consistently projected changes under mid-century climate scenarios (Palazzi et al., 2013; IPCC 2021).

Taken across the full elevational transect, the gradient described here represents a progression from monsoon-cycle limitation at lower elevations to snowmelt-pulse and compound thermal limitation at upper elevations, with a transitional multi-season moisture integration zone in between. This pattern is consistent with the findings of elevation-stratified studies elsewhere in the Himalayan arc (Gaire et al., 2017; Sigdel et al., 2018) and reflects the ecological plasticity of *P. roxburghii* — its capacity to express different dominant limiting mechanisms across its wide altitudinal range. However, this plasticity also creates compound vulnerability: warm, dry spring conditions that simultaneously reduce snowmelt and pre-monsoon rainfall would depress growth across all elevation bands at once, as appears to have occurred during the synchronous growth suppressions of 2000–2002 and 2018–2021 visible in all three chronologies.

5. Conclusions

Pinus roxburghii across the Lesser Himalayan elevational gradient (400–1,500 m) in northern Pakistan exhibits a universal positive growth response to March precipitation and a universal negative response to March temperature, confirming that thermal amplification of the pre-monsoon moisture deficit is the dominant growth constraint for this species, irrespective of elevation. Beyond this shared signal, elevation systematically restructures the dominant limiting mechanism: lower elevations are additionally constrained by monsoon-season rainfall variability; middle elevations integrate multi-season soil moisture legacies and extended heat stress; and upper elevations are governed by the sequential snowmelt-precipitation moisture pulse combined with compound multi-year thermal vulnerability.

Three practical implications follow for regional forest management. First, late-winter and early-spring moisture availability is the primary determinant of annual forest productivity across the entire elevational range, making watershed protection and pre-monsoon moisture conservation the most broadly effective management targets. Second, upper-elevation stands face the most severe combined risk under continued warming — from shrinking snowpack, earlier melt timing, and elevated evaporative demand operating across multiple seasonal windows — and should be prioritized in conservation and monitoring programs. Third, the synchronous growth suppressions observed during recent monsoon-deficit periods (2000–2002, 2018–2021) across all three chronologies warrant continued systematic monitoring, as projected increases in monsoon variability (IPCC 2021) may make such compound drought events more frequent.

Three research priorities should be addressed in future work: (1) sampling of older trees, remnant snags, and deadwood to extend chronologies beyond 100 years and enable multi-decadal climate reconstruction; (2) acquisition of downscaled or station-derived elevation-specific climate data to allow genuinely band-resolved correlation analyses; and (3) formal fire-year identification with sensitivity analyses to assess the influence of fire-affected ring segments on reported climate signals. Together, these advances would position *P. roxburghii* networks in the Pakistani Lesser Himalayas as a substantial contribution to regional palaeoclimate reconstruction efforts.

Declarations

1. Author Contribution Statement

Mehvish Majeed: Conceptualization, Methodology, Formal analysis, Writing - Original Draft.

Eman Majeed: Data curation, Investigation, Visualization, Writing - Review & Editing.

Dr. Sahar Abidi: Validation, Writing - Review & Editing.

Dr. Sher Shah: Resources, Investigation, Writing - Review & Editing.

Dr. Sohaib Muhammad: Validation, Writing - Review & Editing.

2. Declaration of Competing Interest (Conflict of Interest Statement)

The authors declare that they have no known competing financial interests or personal relationships that could have appeared to influence the work reported in this paper.

Data Availability Statement

Raw ring-width measurement files and standardised chronologies will be submitted to the International Tree-Ring Data Bank (ITRDB; https://www.ncei.noaa.gov/products/paleoclimatology/tree-ring) upon acceptance. CRU-TS 4.08 data are freely available at https://crudata.uea.ac.uk/cru/data/hrg/. R analysis scripts are available from the corresponding author on request.

Acknowledgements

The lead author thanks Bjorn Gunther for supervision and mentorship during this project. Sincere thanks are extended to Raja Muhammad Umer, Inspector General of Forests at the Ministry of Climate Change, Pakistan, for facilitating field access. The authors are grateful to Prof. Dr. Thorsten True, Prof. Dr. Ramzi Touchan, and Prof. Dr. David Meko for academic guidance. CRU-TS 4.08 climate data were provided by the Climatic Research Unit, University of East Anglia.

References

1. Ahmed M, Khan N, Wahab M (2010) Climate response function analysis of Abies pindrow (Royle) Spach. Preliminary results. Pak J Bot 42(1):165–171
2. Ahmed M, Shaukat SS, Siddiqui MF (2011) A multivariate analysis of the vegetation of Cedrus deodara forests in Hindu Kush and Himalayan ranges of Pakistan: evaluating the structure and dynamics. Turkish J Bot 35(4):419–438
3. Barry RG (2008) Mountain weather and climate. In *Mountain Weather and Climate, Third Edition* (pp. 1-506)
4. Bhuju DR, Gaire NP (2012) Influence of climate on radial growth of *Pinus roxburghii* at two forest sites in central Nepal. Banko Janakari 22(2):38–44. https://doi.org/10.3126/banko.v22i2.9191
5. Borgaonkar HP, Pant GB, Rupa Kumar K (1996) Ring-width variations in *Cedrus deodara* and its climatic response over the western Himalaya. Int J Climatol 16(11):1409–1422. https://doi.org/10.1002/joc.3370161205
6. Briffa KR, Jones PD (1990) Basic chronology statistics and assessment. In: Cook ER, Kairiukstis LA (eds) Methods of Dendrochronology: Applications in the Environmental Sciences. Springer, pp 137–152
7. Bunn AG (2008) A dendrochronology program library in R (dplR). Dendrochronologia 26(2):115–124. https://doi.org/10.1016/j.dendro.2008.01.002
8. Cook ER (1985) *A Time Series Analysis Approach to Tree-Ring Standardization*. PhD dissertation, University of Arizona

9. Cook ER, Kairiukstis LA (eds) (1990) Methods of Dendrochronology: Applications in the Environmental Sciences. Springer
10. Cook ER, Seager R, Cane MA, Stahle DW (2007) North American drought: Reconstructions, causes, and consequences. Earth Sci Rev 81(1–2):93–134
11. Fritts HC (1976) Tree Rings and Climate. Academic
12. Gaire NP, Bhuju DR, Koirala M, Carrer M (2017) Site- and species-specific treeline responses to climatic variability in eastern Nepal Himalaya. Dendrochronologia 44:96–107. https://doi.org/10.1016/j.dendro.2017.04.001
13. Harris I, Osborn TJ, Jones P, Lister D (2020) Version 4 of the CRU TS monthly high-resolution gridded multivariate climate dataset. Sci Data 7(1):109. https://doi.org/10.1038/s41597-020-0453-3
14. IPCC (2021) Climate Change 2021: The Physical Science Basis. Contribution of Working Group I to the Sixth Assessment Report of the Intergovernmental Panel on Climate Change. Cambridge University Press
15. Kazmi AH, Jan MQ (1997) Geology and Tectonics of Pakistan. Graphic
16. Khan N, Ahmed M, Khan A (2013) Growth-climate response of Himalayan moist temperate forests from Pakistan: A dendrochronological approach. Dendrobiology 69:23–31. https://doi.org/10.12657/denbio.069.003
17. Khan SR, Ahmed M, Saeed A (2021) Dendrochronology of Chir Pine (*Pinus roxburghii*) in the sub-Himalayan forests of Pakistan: Impact of climate change on tree growth. Environ Monit Assess 193(7):451. https://doi.org/10.1007/s10661-021-09180-9
18. Nehrbass-Ahles C, Babst F, Klesse S, Nötzli M, Bouriaud O, Neukom R, Frank DC (2014) The influence of sampling design on tree-ring-based climate reconstructions. Nat Clim Change 4(9):716–721. https://doi.org/10.1038/nclimate2240
19. Palazzi E, von Hardenberg J, Provenzale A (2013) Precipitation in the Hindu-Kush Karakoram Himalaya: Observations and future scenarios. J Geophys Research: Atmos 118(1):85–100. https://doi.org/10.1029/2012JD018697
20. Peters RL, Groenendijk P, Vlam M, Zuidema PA (2015) Detecting long-term growth trends using tree rings: A critical evaluation of methods. Glob Change Biol 21(5):2040–2054. https://doi.org/10.1111/gcb.12826
21. Core Team R (2023) R: A Language and Environment for Statistical Computing. R Foundation for Statistical Computing, Vienna. https://www.R-project.org/
22. Schweingruber FH (1988) Tree Rings: Basics and Applications of Dendrochronology. Springer
23. Shah SK, Shah K, Yadav RR (2014) Ecological amplitude and growth responses of *Pinus roxburghii* along altitudinal gradient in Nepal Himalaya. Dendrochronologia 32(3):227–235. https://doi.org/10.1016/j.dendro.2014.03.002
24. Shah SMI (2009) Geology of Pakistan. Geological Survey of Pakistan
25. Sheikh MI (1993) Trees of Pakistan. Pakistan Forest Institute, Peshawar

26. Shekhar C, Bhardwaj SK, Chauhan P (2018) Tree-ring width analysis of *Pinus roxburghii* from western Himalayas: Influence of temperature and precipitation on radial growth. Clim Change 148(1–2):143–156. https://doi.org/10.1007/s10584-018-2190-4
27. Sigdel SR, Dawadi B, Camarero JJ, Liang E (2018) Moisture-limited tree growth for a century in western Nepal Himalaya. Agric For Meteorol 249:181–189. https://doi.org/10.1016/j.agrformet.2017.11.027
28. Singh J, Yadav RR, Park WK (2011) Tree-ring-based hydrological records for western Himalaya, India, since AD 1560. Clim Dyn 36(6):1413–1420. https://doi.org/10.1007/s00382-010-0842-4
29. Stokes MA, Smiley TL (1968) An Introduction to Tree-Ring Dating. University of Chicago Press
30. Wigley TML, Briffa KR, Jones PD (1984) On the average value of correlated time series, with applications in dendroclimatology and hydrometeorology. J Climate Appl Meteorol 23(2):201–213. https://doi.org/10.1175/1520-0450(1984)023%3C0201:OTAVOC%3E2.0.CO;2
31. Yadav RR, Park WK, Singh J (2017) Pre-monsoon precipitation variability in Himachal Pradesh, India, over the past millennium. Quatern Int 444:88–94. https://doi.org/10.1016/j.quaint.2016.06.014
32. Zang C, Biondi F (2015) treeclim: An R package for the numerical calibration of proxy-climate relationships. Ecography 38(4):431–436. https://doi.org/10.1111/ecog.01335

Figures

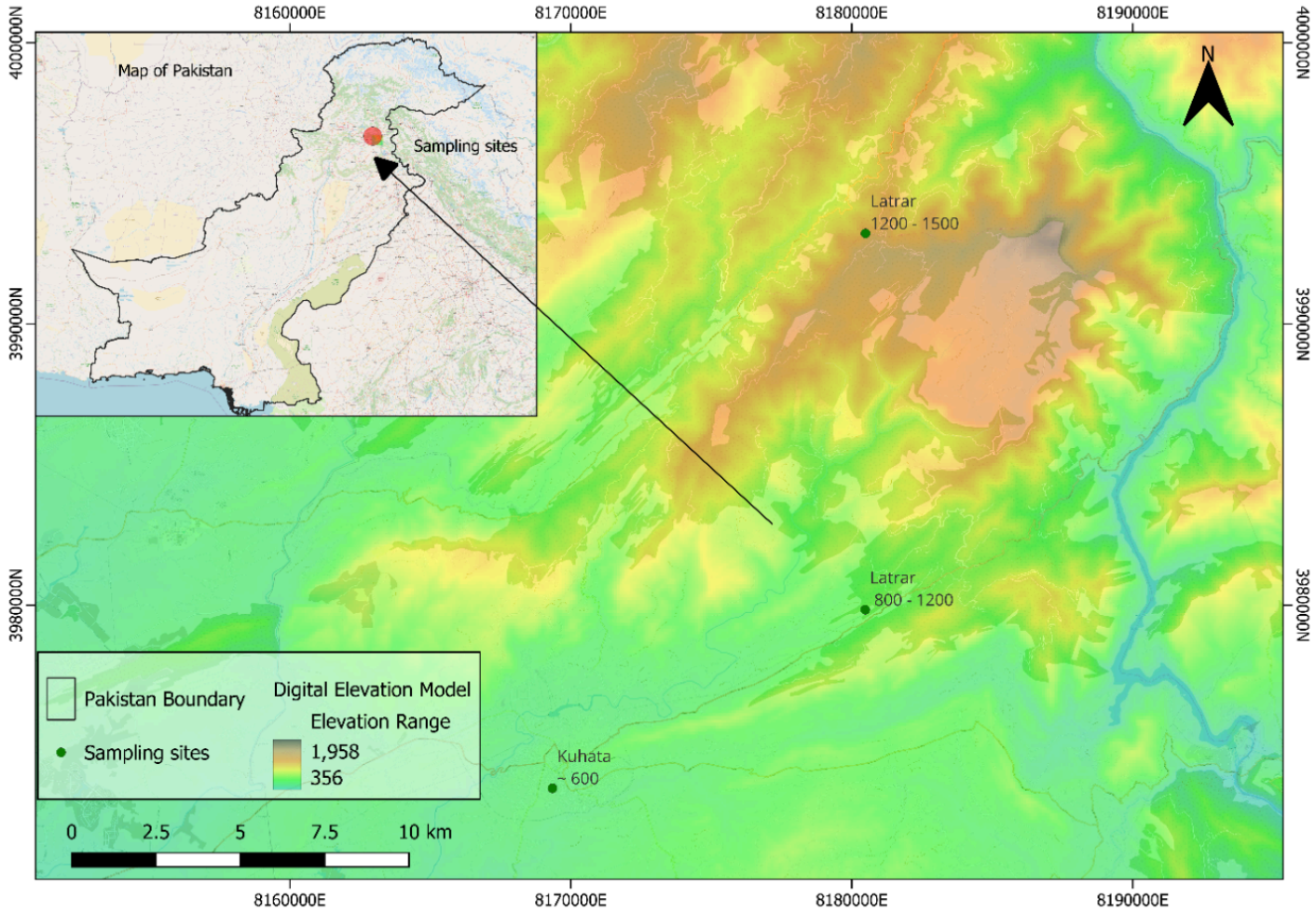


Figure 1

Geographic distribution of *Pinus roxburghii* sampling localities along an elevational gradient in the Lesser Himalayas of northern Punjab, Pakistan. Inset showing the study region within Pakistan. Sampling locations overlaid on a 90-m SRTM Digital Elevation Model (DEM), stratified into the three elevation bands: lower (Kahuta, ~400–800 m), middle (Latrar, 800–1,200 m), and upper (Latrar, 1,200–1,500 m). Colour gradient represents topographic relief.

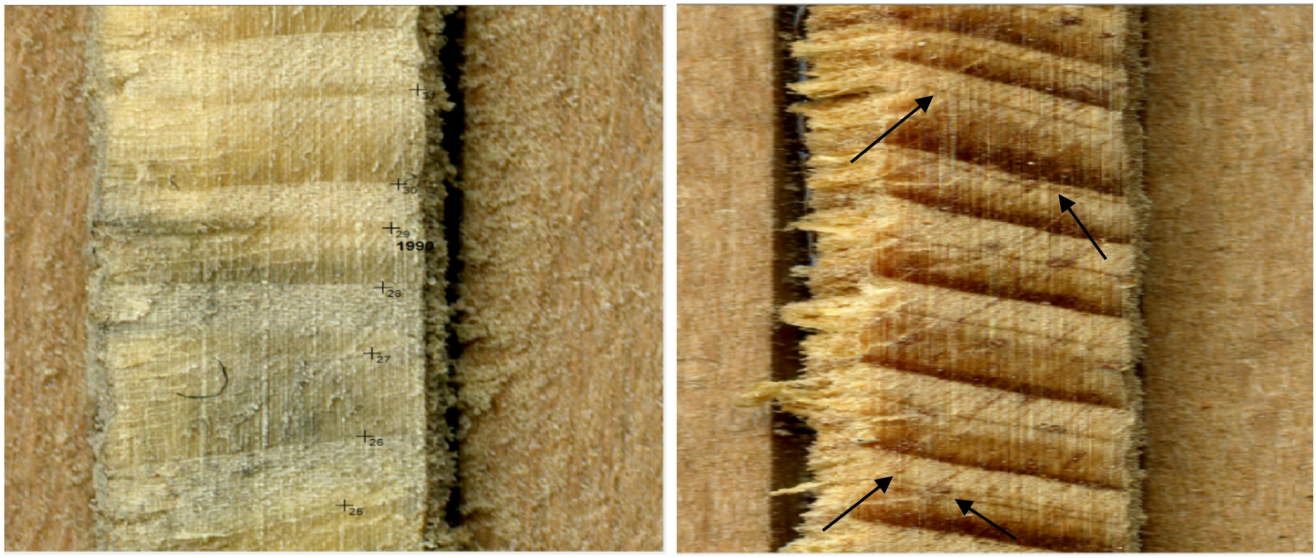


Figure 2

Ring-boundary anomalies in *Pinus roxburghii* cores encountered during cross-dating: (A) faint ring boundaries caused by heavy resin impregnation; (B) false rings of similar origin, with multiple ring-like structures indicated by arrows. Both anomaly types led to core exclusion.

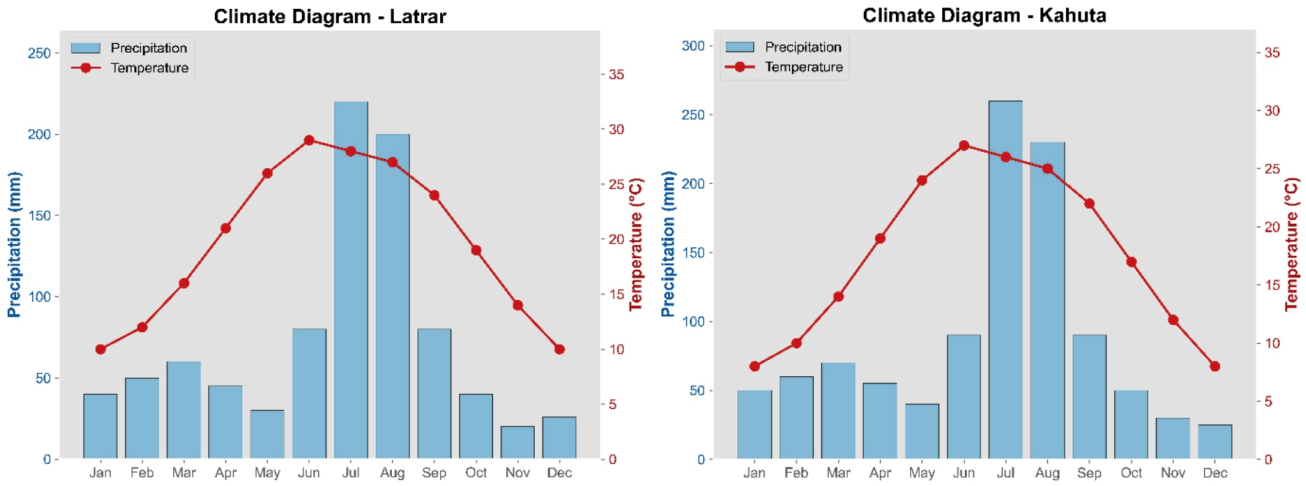


Figure 3

Mean monthly precipitation (bars, left axis) and mean monthly temperature (line, right axis) derived from CRU-TS 4.08 gridded data and local station records for: (A) Latrar (representative of the 800–1,200 m

and 1,200–1,500 m bands); (B) Kahuta (representative of the 400–800 m band). Elevation-band temperature differences at Latrar are addressed by the lapse-rate correction described in Section 2.4.

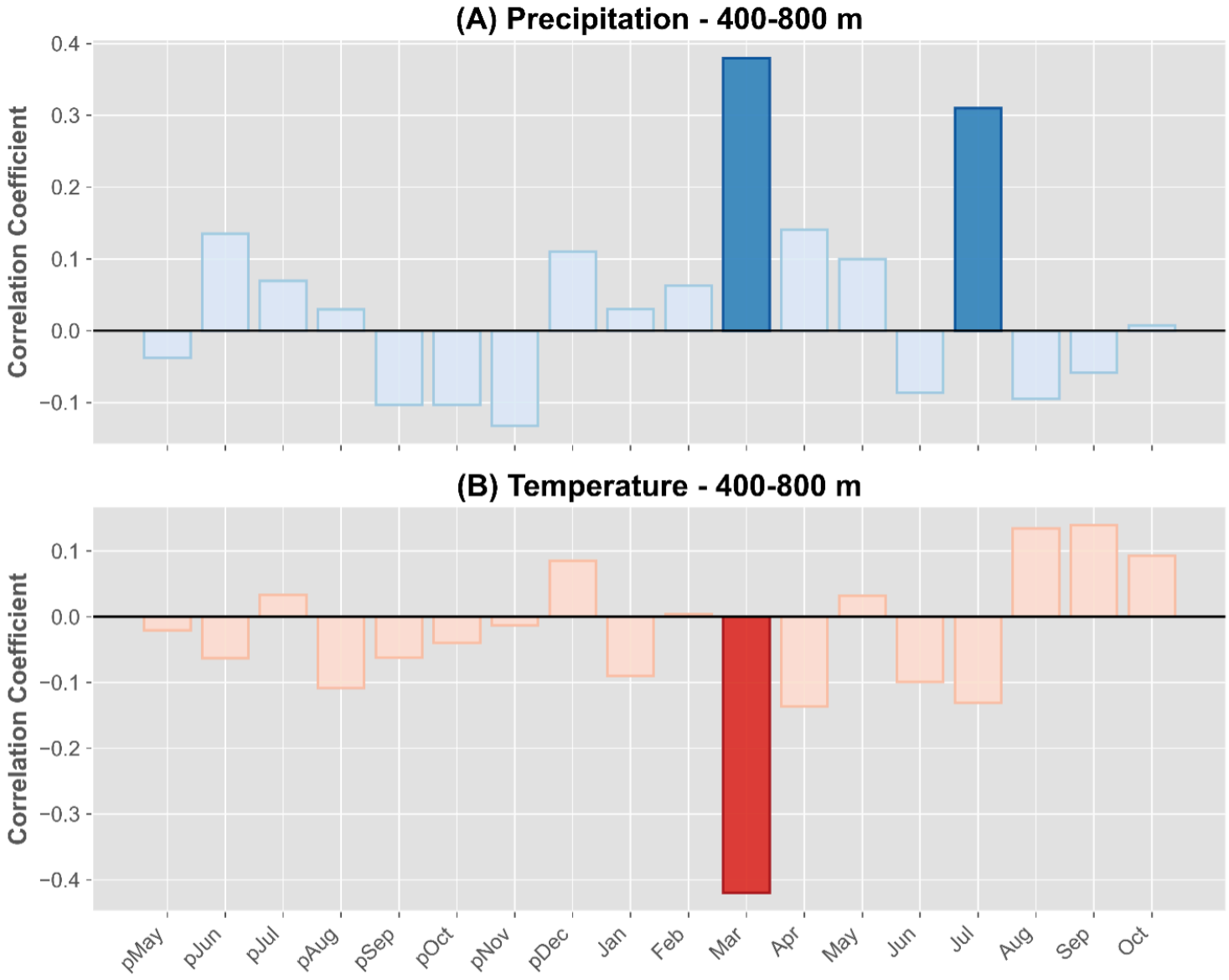


Figure 4

Monthly bootstrapped Pearson correlation coefficients between the standardised ring-width chronology for the lower elevation band (400–800 m, Kahuta; 1952–2021) and (A) monthly precipitation and (B) monthly temperature, from May of the prior year (pMay) through October of the current year (cOct). Filled bars indicate correlations significant at $p < 0.05$ after 1,000-replicate bootstrapping; open bars are non-significant. Error bars show 95% bootstrap confidence intervals. Horizontal dashed lines mark ±0.30.

Image not available with this version

Figure 5

Legend not included with this version

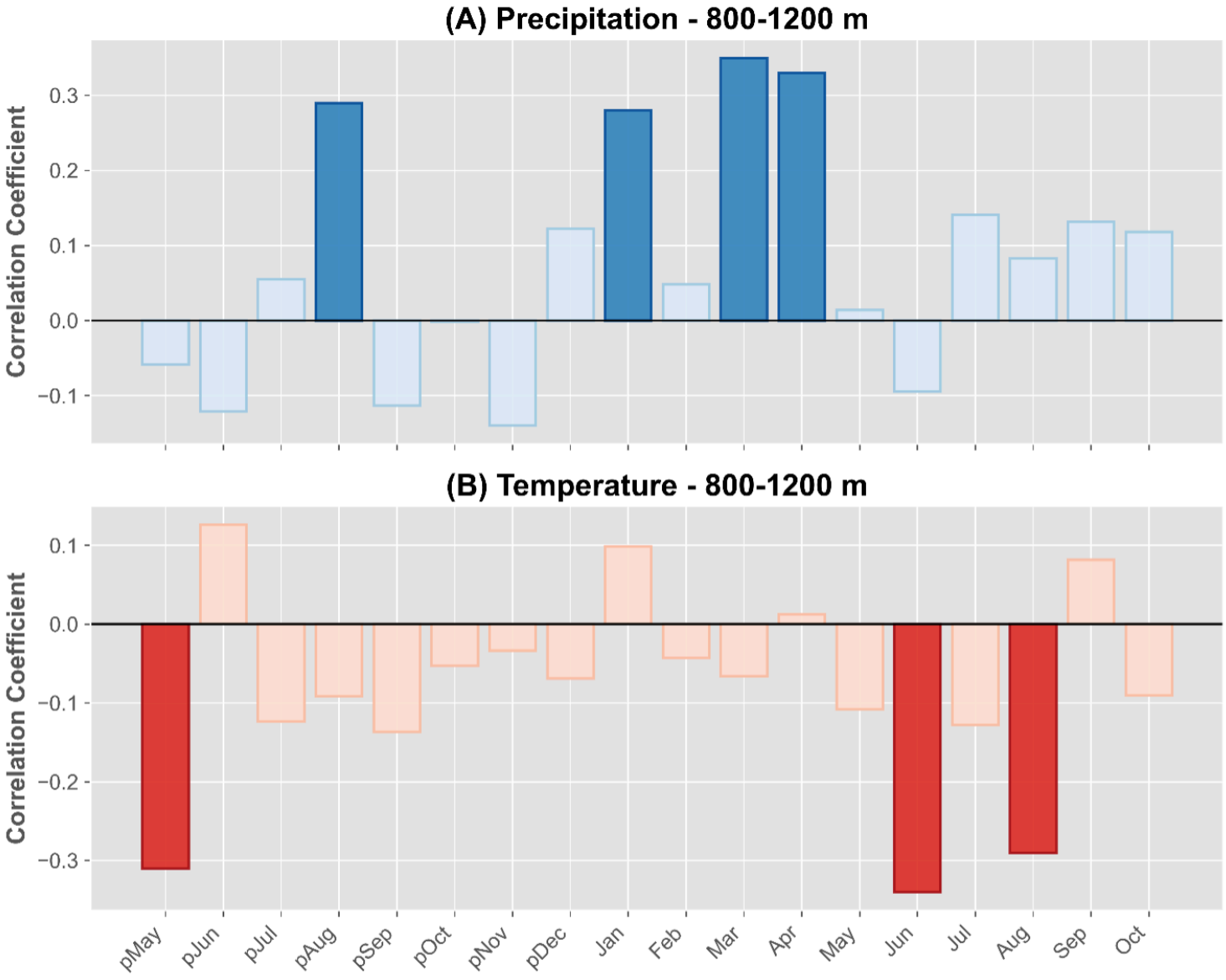


Figure 6

As Figure 6, but for the middle elevation band (800–1,200 m, Latrar; 1934–2021). Rbar = 0.237 at this band is below the commonly applied 0.30 threshold (Table 2); correlations should be interpreted accordingly.

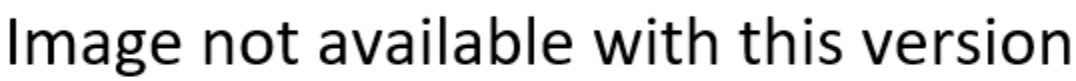


Figure 7

Legend not included with this version

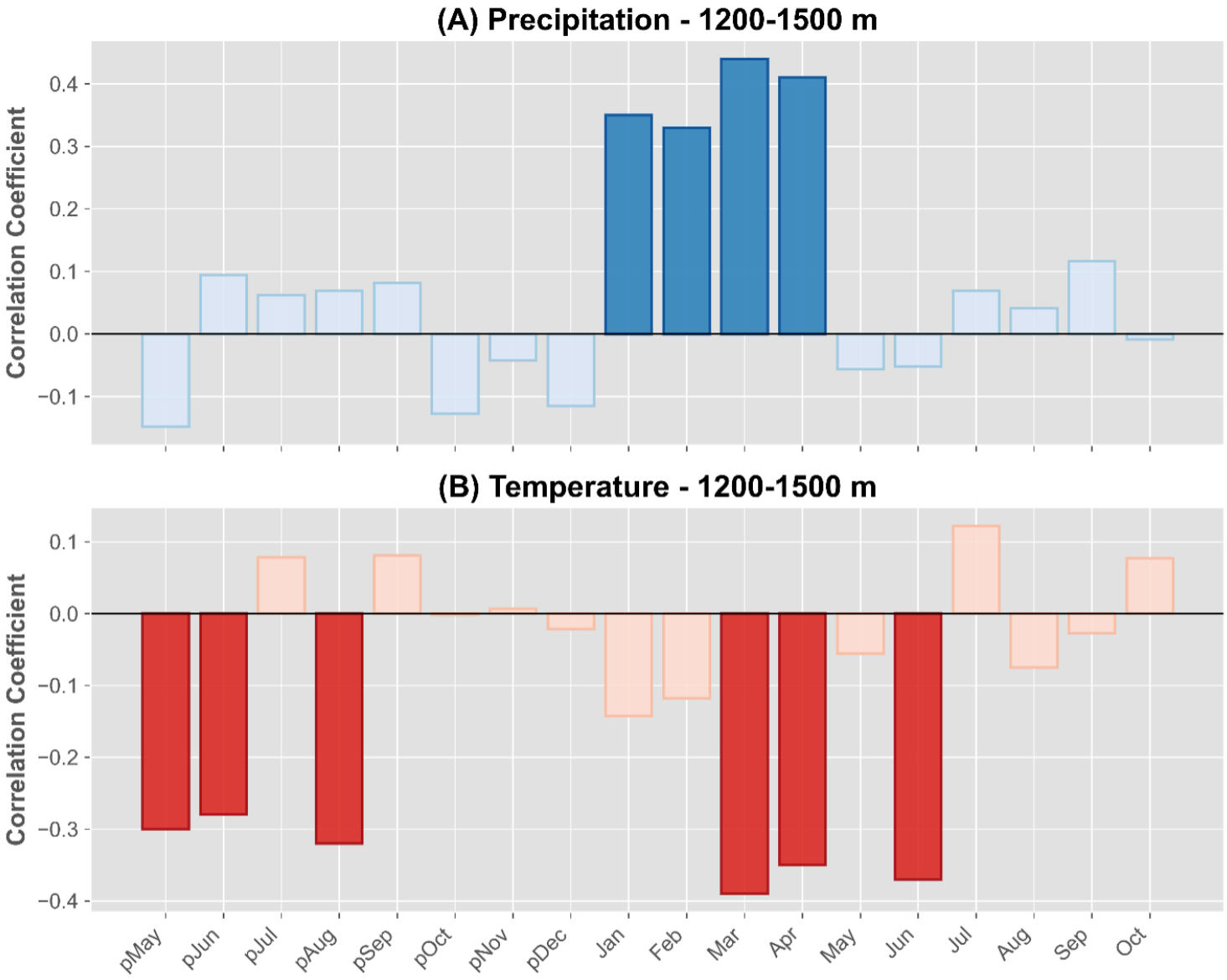


Figure 8

As Figure 6, but for the upper elevation band (1,200–1,500 m, Latrar; 1934–2021).